On the Nature of Murine Radiation-Induced Subcapsular Cataracts: Optical Coherence Tomography-Based Fine Classification, In Vivo Dynamics and Impact on Visual Acuity

Authors: Pawliczek, Daniel, Fuchs, Helmut, Gailus-Durner, Valerie, de Angelis, Martin Hrabê, Quinlan, Roy, et al.

Source: Radiation Research, 197(1) : 7-21

Published By: Radiation Research Society

URL: https://doi.org/10.1667/RADE-20-00163.1

RADIATION RESEARCH **197**, 7–21 (2022)
0033-7587/22 $15.00

DOI: 10.1667/RADE-20-00163.1

On the Nature of Murine Radiation-Induced Subcapsular Cataracts: Optical Coherence Tomography-Based Fine Classification, *In Vivo* Dynamics and Impact on Visual Acuity

Daniel Pawliczek,[a] Helmut Fuchs,[b] Valerie Gailus-Durner,[b] Martin Hrabê de Angelis,[b,c,d] Roy Quinlan,[e] Jochen Graw[a] and Claudia Dalke[a,1,2]

[a] *Institute of Developmental Genetics and* [b] *German Mouse Clinic, Institute of Experimental Genetics, Helmholtz Zentrum München GmbH - German Research Center for Environmental Health, Neuherberg, Germany;* [c] *Chair of Experimental Genetics, School of Life Science Weihenstephan, Technische Universität München, Freising, Germany;* [d] *German Center for Diabetes Research (DZB), Neuherberg, Germany; and* [e] *Department of Biosciences, School of Biological and Medical Sciences, University of Durham, Durham, United Kingdom*

Pawliczek, D., Fuchs, H., Gailus-Durner, V., Hrabê de Angelis, M., Quinlan, R., Graw, J. and Dalke, C. On the Nature of Murine Radiation-Induced Subcapsular Cataracts: Optical Coherence Tomography-Based Fine Classification, *In Vivo* Dynamics and Impact on Visual Acuity. *Radiat. Res*. 197, 7–21 (2022).

Ionizing radiation is widely known to induce various kinds of lens cataracts, of which posterior subcapsular cataracts (PSCs) have the highest prevalence. Despite some studies regarding the epidemiology and biology of radiation-induced PSCs, the mechanism underscoring the formation of this type of lesions and their dose dependency remain uncertain. Within the current study, our team investigated the *in vivo* characteristics of PSCs in B6C3F1 mice (F1-hybrids of BL6 × C3H) that received 0.5–2 Gy γ-ray irradiation after postnatal day 70. For purposes of assessing lenticular damages, spectral domain optical coherence tomography was utilized, and the visual acuity of the mice was measured to analyze their levels of visual impairment, and histological sections were then prepared in to characterize *in vivo* phenotypes. Three varying *in vivo* phenotype anterior and posterior lesions were thus revealed and correlated with the applied doses to understand their marginal influence on the visual acuity of the studied mice. Histological data indicated no significantly increased odds ratios for PSCs below a dose of 1 Gy at the end of the observation time. Furthermore, our team demonstrated that when the frequencies of the posterior and anterior lesions were calculated at early time points, their responses were in accordance with a deterministic model, whereas at later time points, their responses were better described via a stochastic model. The current study will aid in honing the current understanding of radiation-induced cataract formation and contributes greatly to addressing the fundamental questions of lens dose response within the field of radiation biology.

INTRODUCTION

The atomic bombs that were dropped in Hiroshima and Nagasaki, as well as the Mayak and Chernobyl nuclear disasters, all led to numerous long-term health effects in irradiated victims (*1*). One such health effect was radiation damage to the eye lens (*2*). Findings from previously published epidemiological studies have suggested that, of the main cataract types [nuclear, cortical cataract and posterior subcapsular cataract (PSC)], the latter occurred more frequently than the others (*3, 4*).

This phenomenon is closely correlated with a large number of other factors, including steroid administration (*5*), diabetes or age (*6*). The PSC is a well-known cataract type that has been extensively investigated within human lenses via transmission electron microscopy (*7*). The research team confirmed the tendency of ''migratory cells and of bladder cells (also known as Wedl cells)[3] to accumulate at the edge of the PSC'', observed across earlier investigations (*8*). More importantly however, the team elucidated the fine structure of the PSC-constituting cells: bladder cells possessing degenerating nuclei intermixed with cataractous debris and within higher magnifications a ''variety of globular bodies, and crystalloid arrays of membranes'', at the pole a ''semiliquified mass of debris'' and swollen fiber cells located within the cortex over the PSC. The center of the PSC was described

Editor's note. The online version of this article (DOI: https://doi.org/10.1667/RADE-20-00163.1) contains supplementary information that is available to all authorized users.

[1] Current address: Helmholtz Zentrum München GmbH - German Research Center for Environmental Health, Institute of Metabolism and Cell Death, Neuherberg, Germany.

[2] Address for correspondence: Helmholtz Zentrum München GmbH German Research Center for Envirnomental Health, Ingolstädter Landstr. 1, Neuherberg, D-85764, Germany; email: dalke@helmholtz-muenchen.de.

[3] Personal communication.

as a mixture of extracellular fibrogranular material and cellular debris, filament-filled (tonofilaments) pseudobladder cells and viable migratory cells. The authors hypothesized that the migratory cells located at the pole [hereafter referred to as pseudoepithelial cells, see (*9*)] secrete extracellular material, and possibly lysosomal enzymes.

Anterior subcapsular cataracts (ASCs) have been rarely reported as being associated with ionizing radiation exposure. *Ptch1*$^{+/-}$ form higher levels of ASCs after irradiation with at least 3 Gy at postnatal day 2 (*10*). ASCs were additionally reported in mice overexpressing TGFβ (*11, 12*), over the course of an uveitis (*13*), or after irradiation of rats utilizing UV-B light (*14*). ASCs have been described inconsistently as either the formation of epithelial plaques, in which they express a collagenous matrix and then disappear with age (*15, 16*), or as composition of myofibroblastic and ''lens-fiber cell-like'' cells (*17*), whereas there is ongoing discussion as to whether or not the plaque-building cells possessing nuclei are fibroblastic in nature (*18*).

Currently, the International Commission on Radiation Protection (ICRP) asserts that a single ionizing radiation 0.5 Gy dose is capable of typically causing vision-impairing cataracts in men, but only within 1% of the irradiated populace following a postirradiation time period of over 20 years (*19, 20*). To date, the effect of radiation-induced cataracts on murine visual acuity, however, has not yet been examined. Only data collected from mice possessing the same genetic background irradiated at postnatal day 2 are available (*36*).[4] Within the study, inner cortical cataracts were identified and monitored utilizing optical coherence tomography (OCT) and Scheimpflug, and it was demonstrated that these particular lenticular damages were only in part responsible for the massively decreased mean visual acuity measured via the virtual drum. However, no subcapsular cataracts were identified. F. Bettelheim once claimed, ''The most important glare causing cataract is the posterior cataract, which rescatters the already focused light rays'' (*21*). Because our team is aware that type II cataracts [associated with PSCs according to classification (*22*)] are characteristic in mice irradiated approximately 10 weeks after birth, our team assumes the hypothesis that vision impairment via possible PSCs within murine lenses is most likely.

Within the current study, our team analyzed posterior and anterior subcapsular cataracts *in vivo* via the monitoring of murine long-term cohorts utilizing OCT, classified their scattering appearances, matched them with histological structures, and correlated the lenticular and corneal damages with visual acuity data.

[4] This article was accepted after typesetting, therefore this reference is out of order.

MATERIALS AND METHODS

Mice and Irradiations

F1 hybrids of C3HeB/FeJ and C57BL/6JG mice (B6C3F1) were defined as wild types and B6C3F1 mice possessing a heterozygous point mutation within the *Ercc*2 gene *Ercc*2$^{+/S737P}$ as mutants (*23, 24*). Homozygous *Ercc*2 mutants usually form cortical cataracts. By using *Ercc*2$^{+/S737P}$, we sought to investigate a possible influence of a reduced single nucleotide repair on cataract formation after irradiation. A total of 21 mice of each genotype and each sex were sham-irradiated. Then, 20 mice of each genotype and sex received 0.5, 1 and 2 Gy γ-ray irradiation, respectively, via a ^{60}Co source (Eldorado 78 teletherapy irradiator; AECL, Canada). Whole-body-irradiations were performed at a dose rate of 0.3 Gy/min at 10 weeks after birth. Dosimetry was performed using a UNIDOS II dosimeter (secondary electrometer; calibration based upon primary standards of the National Metrology Institute of Germany).

Mice were housed under SPF conditions within the German Mouse Clinic (GMC, https://www.mouseclinic.de) following the German Law of Animal Protection, the ARVO Statement for the Use of Animals in Ophthalmic and Vision Research, and the tenets of the Declaration of Helsinki. All mice were irradiated and examined with the explicit permission of the Government of Upper Bavaria under ROB-55.2-2532.Vet_02-16-167.

OCT and Analysis

An optical coherence tomography of the mouse eye lens was conducted using the Spectralis® OCT (Heidelberg Engineering, Heidelberg, Germany) as described elsewhere (*25*). Retinal analysis was performed as described elsewhere (*26*). Basic technical prerequisites were as follows. A 78-diopter double aspheric lens (Volk Optical Inc., Mentor, OH) was directly affixed on the optical outlet of the device. A second plan-convex contact lens (Roland Consult, Brandenburg, Germany) was reversibly attached to the eyes of the mice utilizing contact media (Methocel 2%; OmniVision, Puchheim, Germany). Mice were anaesthetized using ketamine (100 mg/kg)/xylazine (10 mg/kg). Lenticular OCT was then applied 17.5 months postirradiation within the 0.5 Gy/1 Gy cohorts and 18.5 months postirradiation within the 2 Gy cohort. Additional examinations were performed 13.5 months/14.5 months postirradiation within the 1 and 2 Gy cohort and 10.5 months postirradiation within the 2 Gy cohort. Lenticular phenotypes were classified according the system type listed in Table 1. The type assignment of every lens was not blinded, but unambiguous pictures were discussed among colleagues without knowledge of dose, sex or genetic background.

Scheimpflug

The Scheimpflug system Pentacam® (Oculus GmbH, Wetzlar, Germany) was utilized as described elsewhere (*27*). Mydriasis was induced via 0.5% atropine drops to visualize the lens. To analyze corneal clouding, only frontal pictures were used from the data set. Scheimpflug and OCT data were deposited in STORE^{DB} (DOI: 10.20348/STOREDB/1113/1222).

Visual Acuity Examination

The optokinetic reflex was determined using a virtual optomotor system (Cerebral Mechanics, Lethbridge, Canada) (*28*). The mice were acclimated to room conditions for 30 min prior to examination in the drum to reduce murine agitation. A threshold for visual acuity was determined manually expressed as spatial frequency (*measure/combine* mode) to obtain a comprehensive, whole visual system performance quantity (*29, 30*). For this purpose, measurements started with a base value of just below 0.2 cycles/degree. The threshold was increased or decreased in steps of decreasing value depending on murine movement to approximate the final spatial frequency.

TABLE 1
Distinguished Features of Every Type of the Presented Classification of OCT Images

OCT phenotype	Description
N	Recognizable suture from the pole to the inner cortex. Few scattering center; negligible small areas of depleted signal at the suture.
S	Only areas of enhanced scattering around the suture. Negligible small areas of depleted signal at the suture. Possible layer of increased signal at the posterior pole.
SF	Distinctive area/areas of signal depletion at the pole with poorly scattering fringes. No areas of increased signal around the signal-depleted area and/or few speckles of increased signal in the outer cortex.
SF/S	Ragged area of signal depletion with possible inclusion of an isle displaying increased signal intensities. Signal-increased edges of the signal-free areas. Areas and spots of increased signal intensity around the lesion. Possible layer of increased signal at the posterior pole.

Histological and Immunohistochemical Analysis

The mice were sacrificed, and then the enucleated eyes were fixed in Davidson solution (9:9:6:3; absolute ethanol, distilled water, formaldehyde, acetic acid) for histological purposes and subsequently embedded within Technovit® 8100 (Heraeus Kulzer, Wehrheim, Germany) at either 4, 12 or 20 months postirradiation. Samples were then cut in 2-µm mid-sagittal sections with a glass knife ultramicrotome (OM U 3, C. Reichert, Austria), heat-fixed on superfrost slides, and then stained with basic fuchsin and methylene blue. Slides were then scanned (EVOS® FL Auto Imaging System), and images were contrast-adjusted and background-corrected utilizing the image-processing program, GIMP version 2.8.2.

For purposes of immunohistochemical analysis, eyes were fixed in a 4% PFA-solution for maximal 18 h, dehydrated (infiltration automate TP1020; Leica Biosystems Inc., Lincolnshire, IL), and embedded in paraffin (HistoStar™, Thermo Fisher Scientific™ Inc., Waltham, MA). Samples were then cut (Microtom, Leica), heat-fixed, deparaffined and then rehydrated for standard antigen retrieval, and blocking and blocking protocol. Staining was performed using αA-crystallin [1:400; contributed by Dr. Ales Cvekl, Albert Einstein College of Medicine, Bronx, NY (*31*)], γ-crystallin (1:100; Santa Cruz Biotechnology® Inc., Dallas, TX), and beaded filament structural protein 1 (1:100; contributed by Dr. Roy Quinlan, University of Durham, Durham, UK).

Statistical Analysis

The odds ratios were calculated via multiplication of the quotient of exposed lenses (affected/non-affected) and the quotient of the control lenses (non-affected/affected) as described elsewhere (*32*). To take into account the eventuality of non-affected animals within the denominator, 0.5 was added to every number (*33*). A Mann-Whitney test was conducted using OriginPro®2017. For the purpose of classification of the posterior lens lesions, the fractions of different phenotypes and posterior signal-free area were then calculated for each experimental group by dividing the number of affected lenses by the number of total lenses investigated. Mann-Whitney tests for hypothesis testing on two samples were performed using OriginPro® 2017. Significance was established at $P = 0.05$ (*), $P = 0.01$ (**) and $P = 0.001$ (***).

Experimental Flow

Mice were examined utilizing the Scheimpflug camera each month, beginning with one month postirradiation. In tandem, all mice were additionally examined using OCT after every 4 months, beginning 3 months postirradiation (0.5 and 1 Gy cohort plus associated controls) or beginning 4 months postirradiation (2 Gy cohort and associated controls). Visual acuity was determined 18–19 months postirradiation. Mice were sacrificed 20 months postirradiation for histology purposes and immunohistochemical analysis. Additional mice not employed for long-term investigation purposes were sacrificed 4 and 12 months postirradiation for histological purposes.

RESULTS

Posterior Lens Lesion In Vivo Classification

Independent of the applied dose at the initial irradiation, four varying posterior lens phenotypes were observed *in vivo* with OCT over time (Fig. 1). One particular phenotype was characterized with minor flecks of opacification, or with no opacification at all, and a clearly visible suture structure (Fig. 1A), thus the designation ‘‘normal’’ (N) was provided in these occurrences. Apart from this minimum of changes in the lens, two phenotypes of basic alterations emerged among the samples: the phenotype possessing clustered scattering structures around the suture (Fig. 1B), demarcated with ‘‘scattering’’ (S) and one phenotype with a posterior signal-depleted area at the suture (Fig. 1C), demarcated with ‘‘signal-free’’ (SF). These basic phenotypes of clear alterations were typically observed combined

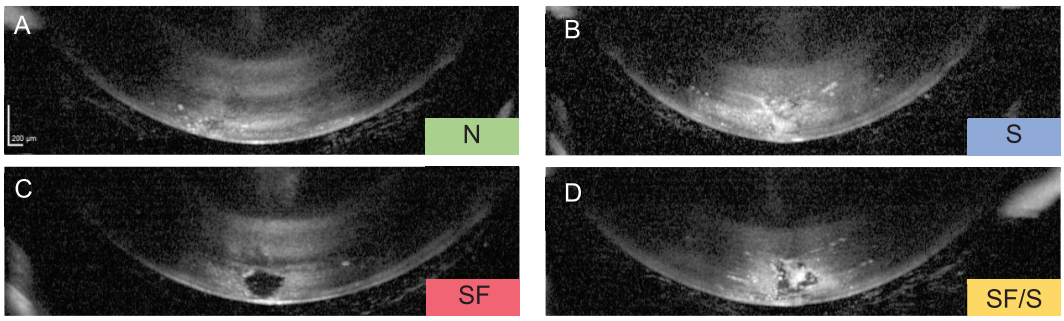

FIG. 1. Phenotypes observed *in vivo* utilizing optical coherence tomography 17.5–18.5 months postirradiation. Panel A: Normal type (N) exhibiting no obvious alterations. Panel B: Scattering phenotype (S) exhibiting massive scattering center. Panel C: Phenotype with signal-free (SF) area. Panel D: Combined phenotype (SF/S) with characteristics of SF- and S-type lesions.

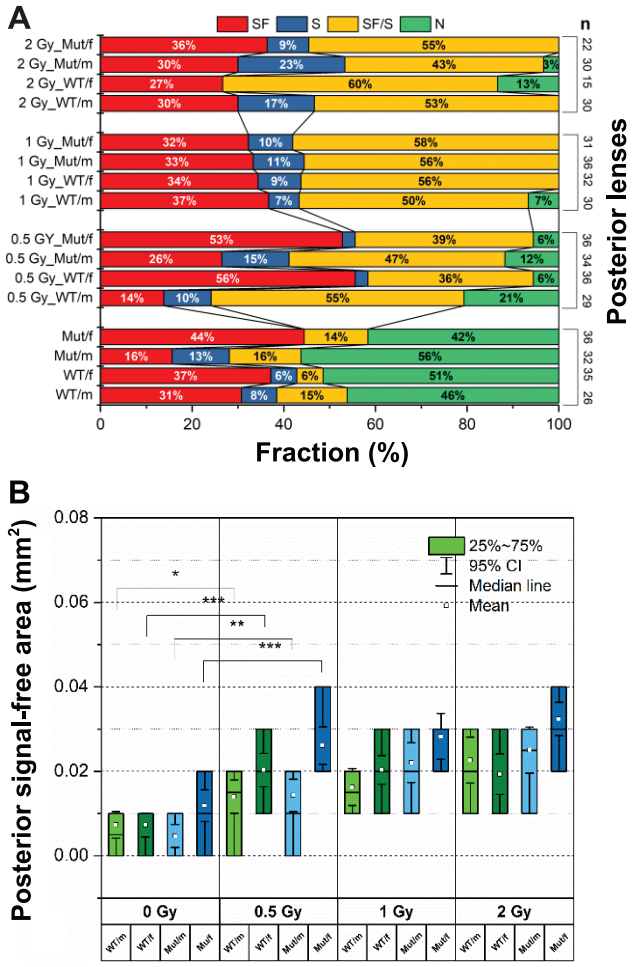

FIG. 2. Distribution of posterior *in vivo* phenotypes 17.5–18.5 months postirradiation, imaged via optical coherence tomography (panel A). Fraction of control phenotype (N, green), signal-free/scattering type lesions (SF/S, yellow), scattering type lesions (S, blue) and signal-free type lesions (SF, red); n = number of lenses. Posterior signal-free area of SF and SF/S-type lesions, 17.5–18.5 months postirradiation for all groups and doses applied (panel B). Statistical significances were determined using Whitney-Mann test.

(Fig. 1D), and were designated accordingly as ''SF/S'' (see also Table 1).

As expected, posterior lesions were identified as spatial phenomena. Volume scans across all phenotypes revealed the dimensions of those lesions and their consistency. Lesions barely exceeded 200 μm following the optic axis, measured from the posterior end to the nucleus, and 500 μm following the dorsal-to-cranial axis, which renders the lesions pure outer cortical phenotypes. Lesions of the S-type enclosed no caverns of signal-free areas. If they did, they were SF/S-type lesions. In 3-dimensional analysis, this type classically displayed an enclosure of a scattering isle along all sides by a signal-free area (e.g., Fig. 1D). Occasionally, this phenotype was increasingly more ragged alongside lateral-spreading signal-free areas. SF-type lesions, on the other hand, were free of any scattering within the entirety of their volume (volume scans of all types in Supplementary Data,

TABLE 2
The Odds Ratios of Posterior *In Vivo* Phenotypes Imaged Using Optical Coherence Tomography 17.5–18.5 Months Postirradiation (Groups Pooled for Every Cohort)

Phenotype	Comparison	Odds ratio	95% CI	*P* value
SF/S	0.5 Gy vs. 0 Gy	**5.4**	2.93–10.23	<0.001
	1 Gy vs. 0 Gy	**8.64**	4.61–16.20	<0.001
	2 Gy vs. 0 Gy	**7.51**	3.89–14.50	<0.001
S	0.5 Gy vs. 0 Gy	1.2	0.46–3.16	0.69
	1 Gy vs. 0 Gy	1.55	0.61–3.93	0.35
	2 Gy vs. 0 Gy	**2.55**	1.02–6.35	0.04
SF	0.5 Gy vs. 0 Gy	1.29	0.78–2.15	0.31
	1 Gy vs. 0 Gy	1.07	0.63–1.79	0.79
	2 Gy vs. 0 Gy	0.92	0.52–1.63	0.79
	0.5 Gy vs. 0 Gy	0.12	0.06–0.23	<0.001
N	1 Gy vs. 0 Gy	0.01	0.003–0.069	<0.001
	2 Gy vs. 0 Gy	0.03	0.01–0.11	<0.001

Phenotype	Comparison	Fraction (%)	Odds ratio	*P* value
S + SF + SF/S	0 Gy	51.6	1	
	0.5 Gy vs. 0 Gy	89.6	**8.26**	<0.001
	1 Gy vs. 0 Gy	98.4	**60.6**	<0.001
	2 Gy vs. 0 Gy	96.9	**29.9**	<0.001

Note. Significantly altered ratios were demarcated by boldface font.

Videos S1–4; https://doi.org/10.1667/RADE-20-00163.1.S1; https://doi.org/10.1667/RADE-20-00163.1.S2; https://doi.org/10.1667/RADE-20-00163.1.S3; https://doi.org/10.1667/RADE-20-00163.1.S4, respectively).

The distribution of introduced phenotypes was characteristic for controls and irradiated mice, respectively (Fig. 2A). The lenses of mice that received 0.5 Gy and increased doses exhibited a much larger fraction of the combined SF/S-lesion type when contrasted with controls expressed via significantly increased odds ratios (Table 2, SF/S). The S-type was significantly increased solely for the 2 Gy cohort (Table 2, S). Control lenses, in contrast, were not affected in at least 42% (female mutants) of any group. Within the 1 and 2 Gy cohorts, the N-type disappeared across almost every group (2 Gy irradiated female WT might be an outlier because of low survival; the implications of this are further addressed in the Discussion below). Also of note is that the controls as well as the irradiated murine lenses exhibited a baseline frequency of SF-type lesions (no significant differences were observed between the cohorts). That observation was altered by the fact that the size of the signal-free area of those types of lesions was dependent upon the previous irradiation (e.g., SF size in controls 0.019 mm^2 and 0.025 mm^2 in 2 Gy irradiated mice, 17.5–18.5 months postirradiation, $P = 0.01$).

The average posterior signal-free area (PSFA) of mice that received 0.5 Gy was at least twice as large as within any of the control groups at 17.5–18.5 months postirradiation (Fig. 2B), although the differences between the 0.5, 1 and 2 Gy irradiated groups were not significant at 17.5–18.5 months postirradiation. This was not necessarily the case at

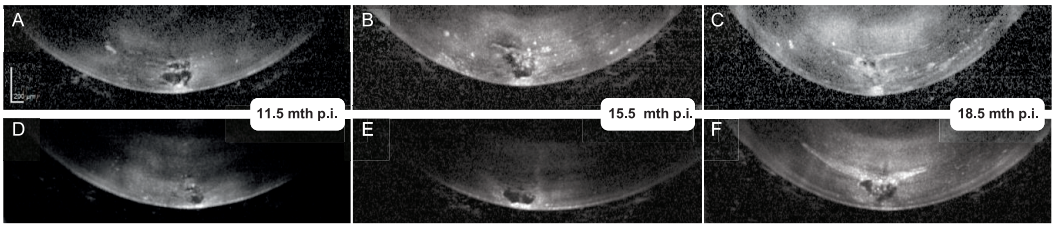

FIG. 3. Examples for posterior lesion dynamics monitored via optical coherence tomography. Panels A–C: Lenses of a 2 Gy irradiated male WT. Panels D–F: Lenses of a female mutant control. p.i. = postirradiation.

prior time points. For example, all mice of the 2 Gy cohort possessed significantly higher average PSFA four months earlier [average cohort PSFA of 0.036 mm^2 within 95% CI (0.03–0.041) vs. 0.025 mm^2 within 95% CI (0.019–0.029)].

Posterior Lesion Dynamics

Across all three irradiated cohorts several instances of dynamic lesions were easily monitored. They had in common a SF- or SF/S-type lesion (Fig. 3A–C) altered to a purely S-type lesion (under loss of the signal-free area), or at least to a SF/S-type lesion with an additional scattering layer vertical to the posterior suture (Fig. 3D–F). The development of this phenotype was observed within 3.8% of all control and within 5.5% of all irradiated lenses.

Anterior Lesions In Vivo

Anterior lesions, observed within the 2 Gy irradiated cohorts, were similar in appearance to the posterior lesions, as long as they were directly located beneath the anterior capsule (Fig. 4C). Removed from this relationship, anterior lesions could reach much deeper into the cortex than posterior lesions. In some cases, signal-free areas reached deeper than 200 μm into the anterior cortex, while no affected lens fiber cells formed the lens suture beneath the capsule (Fig. 4D). Those deeper-reaching lesions were characterized by a surrounding area of increased scattering (Fig. 4D, red arrow), highly dissimilar from the punctual scattering center within the posterior lens. In addition, deeper-reaching scattering layers could appear between the anterior lesions and the lens nucleus without signal-free caverns located within the vicinity (Fig. 4C and D, green arrows). Deep anterior cortical scattering was also occasionally identified within the controls of the same age (Fig. 4A, green arrow).

The breakdown of the anterior lesion types in OCT revealed a slightly different makeup compared to the posterior lesion analysis: the majority of lenses were of the SF/S-type, but less SF- and more N- types were observed (Fig. 5A). In stark contrast to the posterior part of the controls, no anterior lesion was observed within sham-irradiated mice. The average anterior signal-free area (ASFA) across all groups of the cohort was 0.011 mm^2 and thus, less than one half of the PSFA of the 2 Gy cohort (Fig. 5B).

Histological and Immunohistochemical Lesion Analysis

In the overwhelming majority of investigated lenses postmortem, either anterior or posterior lesions at the Y-suture were discernible. Those lesions consisted of either enlarged or liquefied fiber cells, intercellular free spaces, or pseudoepithelial cells (Fig. 6A and E).

By our definition, the appearance of none of the aforementioned features defines an intact lens structure (Fig. 6B and F), one component comprises an irregularity (Fig. 6C and G), whereas a posterior or anterior subcapsular cataract was identified as such if the lesions were composed of at least two of those components or only comprised of fiber cells swollen so that the eventual lesion possessed at least the size of a multicomponent cataract (Fig. 6D and H).

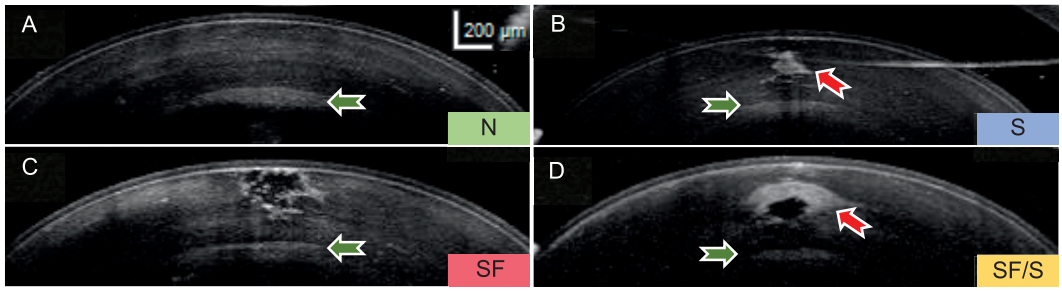

FIG. 4. Variety of anterior lesions 18.5 months after 2 Gy irradiation. Panel A: Normal lens (N) possessing deep reaching scattering layer. Panel B: Scattering type (S) lacking a signal-free area within. Panel C: Anterior signal-free area (SF) with scattering fringe located directly beneath the capsule. Panel D: Combined signal-free/scattering type lesion (SF/S) deep within the anterior cortex with broad-scattering fringe around. Red arrows indicate signal-free area-associated scattering, green arrows indicate signal-increased area within deeper layers.

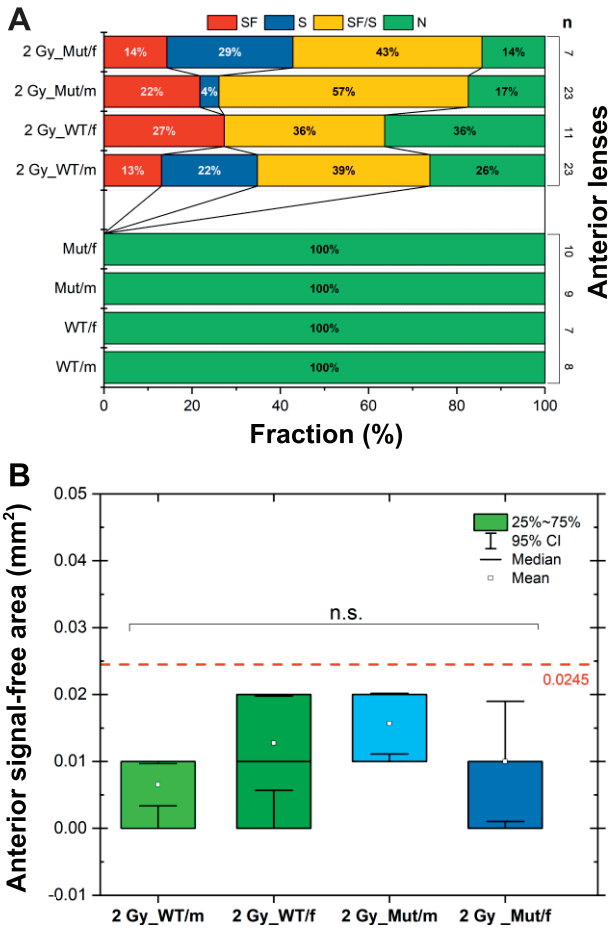

FIG. 5. Distribution of anterior *in vivo* phenotypes 18.5 months after 2 Gy irradiation, imaged with optical coherence tomography (panel A). Fraction of control phenotype (N, green), signal-free/scattering type lesions (SF/S, yellow), scattering type lesions (S, blue) and signal-free type lesions (SF, red). Anterior signal-free area (ASFA) of SF- and SF/S-type lesions, 18.5 months postirradiation across all groups after 2 Gy irradiation; n = number of lenses (panel B). Red line indicates average posterior signal-free area of all 2 Gy irradiated lenses at the same point in time (0.0245 mm^2). Statistical significances were determined using Whitney-Mann test.

No investigated lens displayed a PSC at 4 months postirradiation. Only two samples in the 2 Gy cohort presented irregularities (Fig. 7A, 4 months postirradiation). After 12 months, across all cohorts, including controls, PSCs were discernible; only in the 2 Gy cohort were those PSCs significantly increased in number compared to the controls (Table 3, 12 months postirradiation, 0 Gy vs. 2 Gy). Furthermore, a considerable number of lenses displayed irregularities at this time point. PSC frequencies appeared to be linearly dependent on dose 20 months postirradiation (Fig. 7A), but only the odds ratios concerning PSCs of the 1 Gy and 2 Gy cohort were significantly increased (Table 3, 12 months). Akin to the PSC frequencies, anterior cataracts (ACs) were more frequently found at rates of higher significance within lenses at 20 months after 1 and 2 Gy irradiation (Table 4).

A very low number of cases deviated from the typical phenotype of posterior and anterior lesions (Fig. 8A–C). They displayed an increased accumulation of pseudoepithelial cells as a multi-layered plaque at the anterior suture (Fig. 8A) or as mono- and bilayer at the posterior suture respectively (Fig. 8B). Obvious massive occurrence of intracellular small vacuoles within the anterior lens was observed only 1–2 times across ~120 samples, 20 months postirradiation (Fig. 8C).

Histology made it possible to match OCT-derived posterior phenotypes, solely established via opto-physical properties, with cytological changes within the same lenses (Fig. 9). The N-type in OCT was matched in histology by a nearly regular suture with maximally few, slightly increased swollen fiber cells, and one to two misguided pseudoepithelial cells (Fig. 9A).

The S-phenotype was difficult to identify using histology. Sections of the lens exhibited a large quantity of slightly increased swollen fiber cells at the suture, with a general predominant tendency to direct in a horizontal layer (Fig. 9B). PSCs possessing a large reservoir of liquefied proteins or very few enlarged fiber cells at the suture were apparent within OCT as the SF-phenotype (Fig. 9C). Mature PSCs

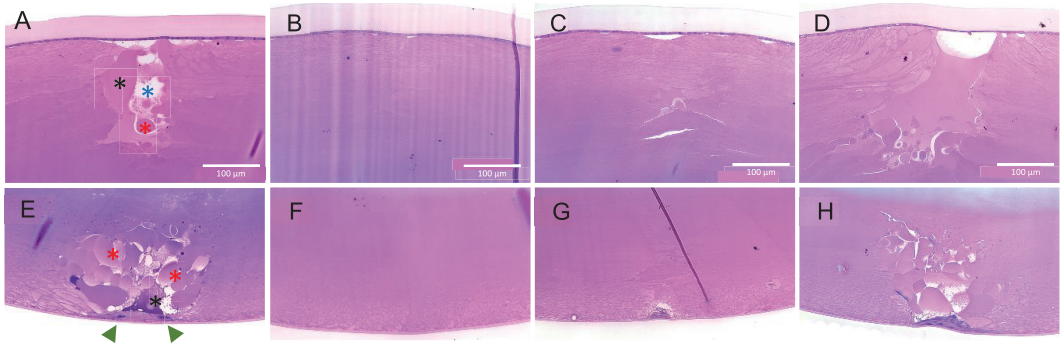

FIG. 6. Representative histological images (40×) of anterior (above) and posterior (below) lens alterations. Possible alterations at the suture were enlarged fiber cells (red stars), liquefied protein reservoirs (black star), intercellular spaces (blue star) and pseudoepithelial cells (green arrowheads) (panels A and E). Unaffected lens (no finding) with regular suture (panels B and F). First irregularities with slightly enlarged fiber cells at the suture and subcapsular pseudoepithelial cells (panels C and G). Posterior subcapsular cataract (panels D and H).

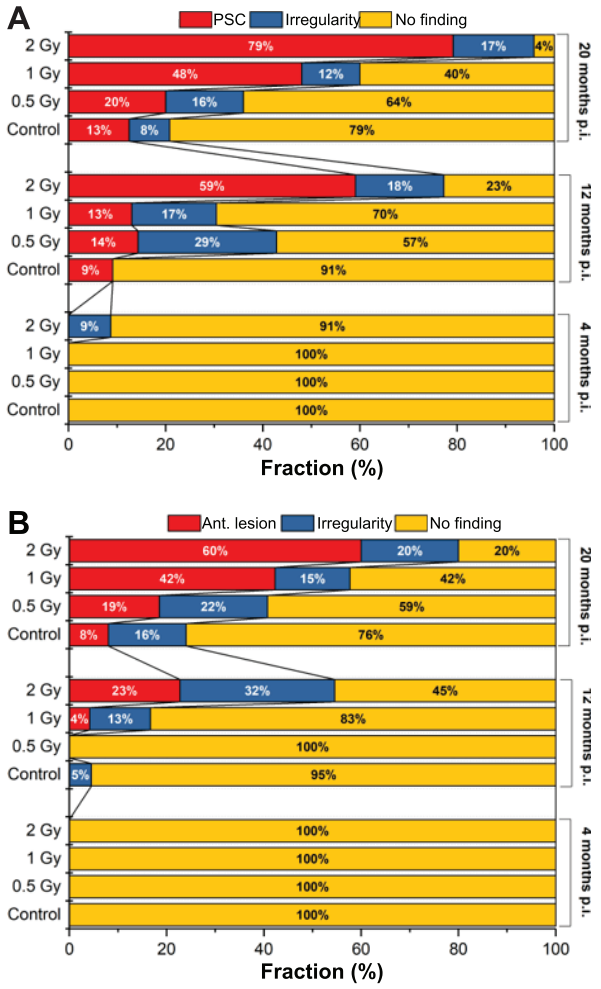

FIG. 7. Distribution of posterior (panel A) and anterior (panel B) lens alterations at 4, 12 and 20 months postirradiation with 0.5, 1 and 2 Gy (sex and genotype pooled). Lenses lacking any alterations (no finding), lenses exhibiting first irregularities (irregularity), posterior subcapsular cataracts (PSC), anterior lesions including anterior subcapsular cataracts (ant. lesions). p.i. = postirradiation.

possessing a fragmented lesion appearance, indicating many irregularly shaped fiber cells, intercellular spaces and possible cellular debris stained via methylene blue, appeared to constitute the SF/S-type within OCT (Fig. 9D). Pseudoepithelial cells beneath the capsule were a feature of both the SF- and the SF/S-type.

The distribution differences of crystallins, which are crucial for transparency and chaperone activity, contributed to elucidate questions regarding the signal-free areas visible within OCT (Fig. 10). Three examples of posterior lenticular lesions of the SF/S-type (Fig. 10, I and III) or the SF-type (Fig. 10, II) were presented. Overall, αA-crystallins were present within the entire fixed cortex (Fig. 10J–L), while γ-crystallins appeared only as a weak signal in the more inner cortex (Fig. 10M–O). As it appeared, the areas devoid of crystallins (Fig. 10J–L, white stars) correlated with the signal-free areas in OCT. As expected via the appearance in the OCT images, the signal-free areas within the SF/S-type lesions were quite fragmented and, within the SF-type lesion, presented as a uniform body. Swollen fiber cells within the lesion (Fig. 10L, yellow star) emitted an αA- crystallin signal at the same level as the surrounding, more regular cells in the same distance to the lesion. Nuclei-containing cells accumulated directly subcapsular (Fig. 10G and I, red arrows) and very few nuclei were spotted within the cortex above the lesion (Fig. 10, I, white arrow). Of high importance was the missing crystallin signal within the cells containing these nuclei (Fig. 10D). The SF-type lesion was nuclei-free (Fig. 10H), and the cells adjacent to the signal-free area were less swollen, and the suture was more typical in appearance (Fig. 10K).

Beaded filament structural protein 1 (BFSP1) distribution within posterior lesions and irregularities were akin to the observed αA- crystallin distribution: there was no detectable signal within the reservoirs (Fig. 11J–L) and the pseudoepithelial cells (Fig. 11D). However, BFSP1 was homogeneously present across the entire fixed outer cortex (Fig. 11D–F).

TABLE 3
The Odds Ratios of Posterior Subcapsular Cataracts Identified in Pooled Histological Analysis (Fig. 7A)

Time postirradiation	Comparison	Odds ratio	95% CI	*P* value
12 months	0.5 Gy vs. 0 Gy	1.57	0.23–10.51	0.63
	1 Gy vs. 0 Gy	1.5	0.22–9.96	0.67
	2 Gy vs. 0 Gy	**14.44**	2.68–77.79	0.002
20 months	0.5 Gy vs. 0 Gy	1.75	0.36–8.30	0.48
	1 Gy vs. 0 Gy	**6.46**	1.52–27.32	0.011
	2 Gy vs. 0 Gy	**26.60**	5.58–126.59	<0.001

Notes. Significantly altered ratios were demarcated by boldface font. No PSCs at 4 months postirradiation.

Corneal Clouding

Lenticular damage was not accompanied by significant retinal changes, but was accompanied by increased opacifications of the cornea (Fig. 12). Clouding was identified by OCT as increased scattering in the cornea and the concurrent signal quenching within the lens (Fig. 12C). Histological sections of these eyes revealed substan-

TABLE 4
Odds Ratios of Anterior Lesions Identified in Pooled Histological Analysis (Fig. 7B)

Time postirradiation	Comparison	Odds ratio	95% CI	*P* value
12 months	1 Gy vs. 0 Gy	2.87	0.11–74.26	0.52
	2 Gy vs. 0 Gy	14.14	0.73–273.40	0.07
20 months	0.5 Gy vs. 0 Gy	2.61	0.45–14.90	0.27
	1 Gy vs. 0 Gy	**8.43**	1.63–43.52	0.01
	2 Gy vs. 0 Gy	**17.25**	3.30–89.97	<0.001

Notes. Significantly increased ratios were demarcated by boldface font. No anterior lesions at 4 months postirradiation.

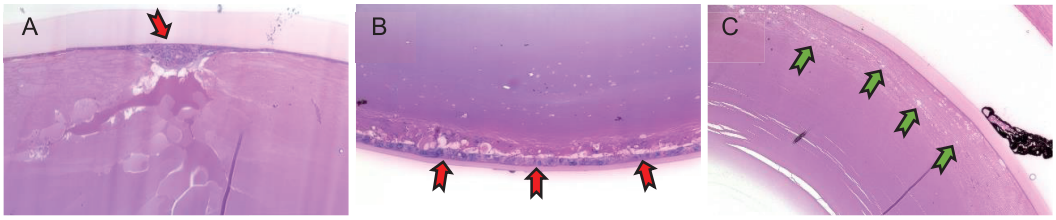

FIG. 8. Non-representative examples of maximal alteration across all lens parts (example from 1 Gy irradiated cohort). Anterior subcapsular cataract with multi-layered pseudoepithelium (red arrow) beneath the regular lens epithelium, 40× (panel A). Standout instance of a posteriorly covering pseudoepithelial layer, 20× (panel B). Lens exhibiting vacuoles (green arrows) between equators and anterior suture, 20× (panel C).

tial alterations in the corneal stroma. Instead of a single fine basal lamina, the affected corneas developed an additional layer that appeared as lamina with several epithelial cells interspersed at the cleft or stroma, filling the space towards the interrupted epithelium (Fig. 12B). Neovascularization (erythrocyte-filled caverns) was discernible within the stroma beneath the pseudo-basal lamina (Fig. 12B).

Within the 2 Gy cohort, the female mutants exhibited higher amounts of corneal alterations (and these alterations could always be detected by OCT): alterations were observed three times more often within this group than within the controls (Table 5, last row). Irradiated male mutants were not at all affected, the same as the controls. Only the female WT were one third as often affected as the controls. We observed that those cornea opacifications appeared very late in the mice's lifetime (~15 months postirradiation).

Visual Acuity

The reduction of mean spatial frequency of the majority of the irradiated groups did not exceed 20% compared to the control mice at the same age, with the exception of the female mutants irradiated with 2 Gy (reduction of ~45%) (Fig. 13A and B). Already, 0.5 Gy caused a statistically significant reduction of the spatial frequency across all irradiated groups, with the exception of the female mutants. Doubling the dose to 1 Gy only exerted a significant additional impairing effect on the male WT mice (Fig. 13A), while quadrupling the dose to 2 Gy only further decreased the spatial frequency within mutants. A three-way analysis of variance (ANOVA) of all investigated mice (factors sex, line and dose with the levels male/female, WT/mut and 0 Gy/0.5 Gy/1 Gy/2 Gy) revealed that all factors exerted a significant effect on mean differences ($P \leq 0.01$), and all possible interactions of these factors, as well (homoscedasticity confirmed).

The combined signal-free area of both eyes of each mouse was plotted exemplarily against the measured visual acuity for each mouse of the 2 Gy irradiated cohort and then subsequently fitted with a linear regression (Fig. 14A). Linear regression delivered an insufficient correlation coefficient ($R = -0.33$) to conclude a correlation between the signal-free area in the lenses and the slight vision impairment within irradiated mice measured. For example, the female mutants irradiated with 2 Gy possessed the worst visual acuity (labeled data points), but lay in essence on a horizontal line.

Plotting the visual acuity of these mice against their combined corneal clouding (female mutants, determined via Scheimpflug camera and evaluated via OCT) though, revealed a statistically sufficient correlation ($R = -0.8$). Animals exhibiting central corneal clouding within both eyes (combined corneal clouding ≥ 4) in particular lacked visual acuity.

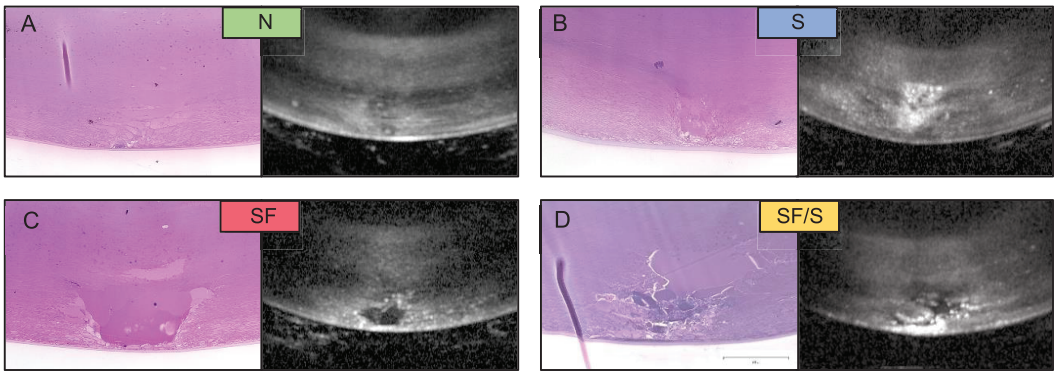

FIG. 9. Assignment of *in vivo* optical coherence tomography (OCT) phenotypes (17.5–18.5 months postirradiation) via matching histological sections (40×) of the same lenses (20 months postirradiation). Panel A: N-phenotype. Panel B: S-phenotype. Panel C: SF-phenotype. Panel D: SF/S-phenotype.

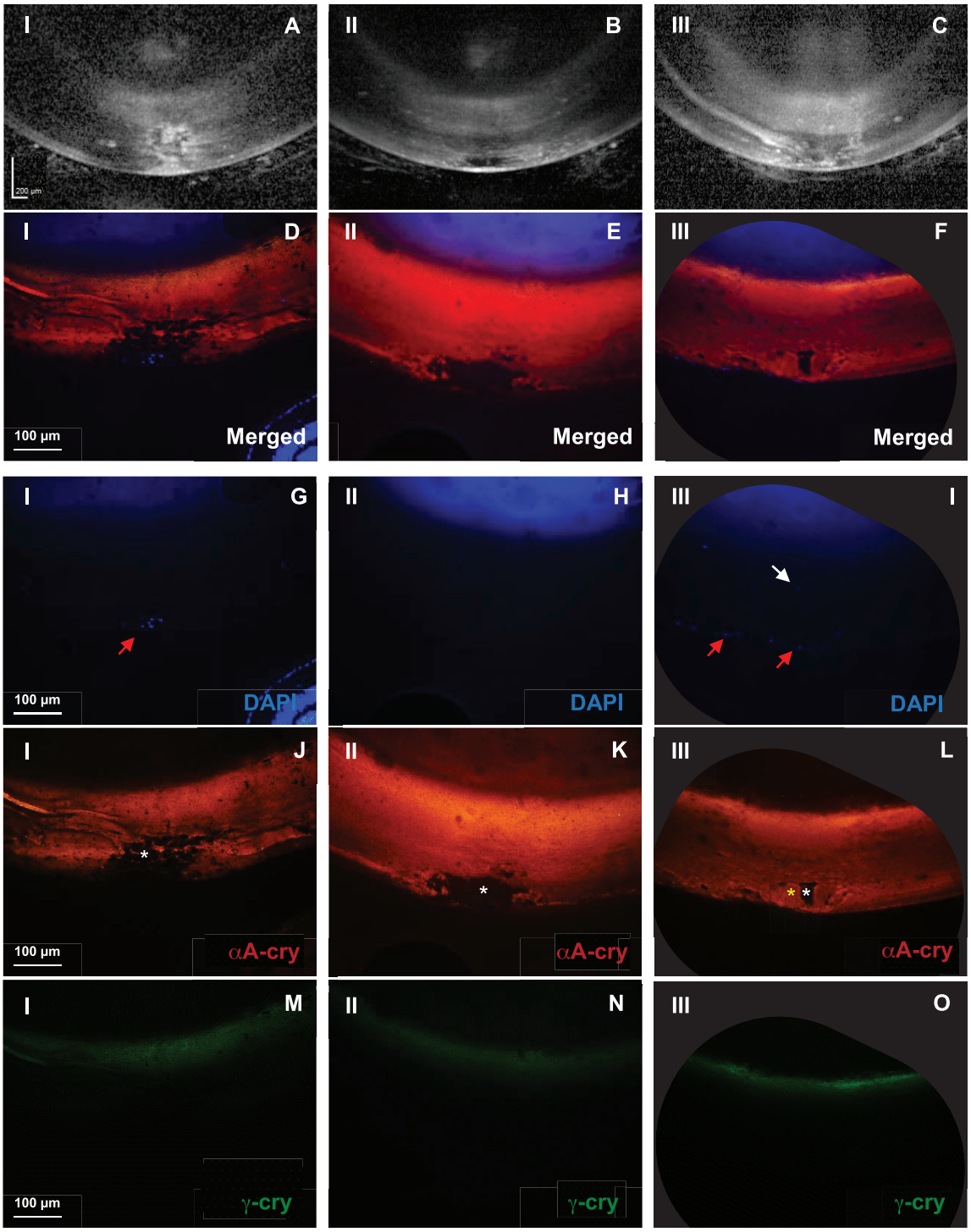

FIG. 10. Lenticular crystallin distribution within posterior lesions of a 2 Gy-irradiated male mutant (I), 0.5 Gy irradiated female mutant (II), and 2 Gy irradiated female WT 20 months postirradiation (III). Panels A–C: OCT image. Panels D–F: Merged IHC image. Panels G–I: DAPI. Panels J–L: αA-crystalline (αA-cry). Panels M–O: γ-crystalline (γ-cry). For panels D–L, magnification = 20×. Red arrows indicate misplaced nuclei. White stars indicate correlates of SF-areas in OCT (tomography not necessarily matching the section). Yellow star indicates swollen fiber cells.

For estimation of the influence of lenticular scattering lesion features upon the eventual outcome in the virtual drum, a posterior scattering score (SS_{post}) was calculated. This score totals the scattering information of both lenses of the mice. Employing a simplistic binary approach, each lesion was counted with 1 if carrying a scattering component (S- and SF/S-types) and 0 if not (N- and SF-type). Accordingly, a mouse with, e.g., two SF/S-type lesions possessed a SS_{post} of 2. The separation of spatial frequencies, e.g., in the 2 Gy cohort, was convincing (Fig. 15A). The mean spatial frequency of mice carrying 2 lenticular lesions with scattering components ($SS_{post} = 2$) was ~15% lower ($P < 0.001$).

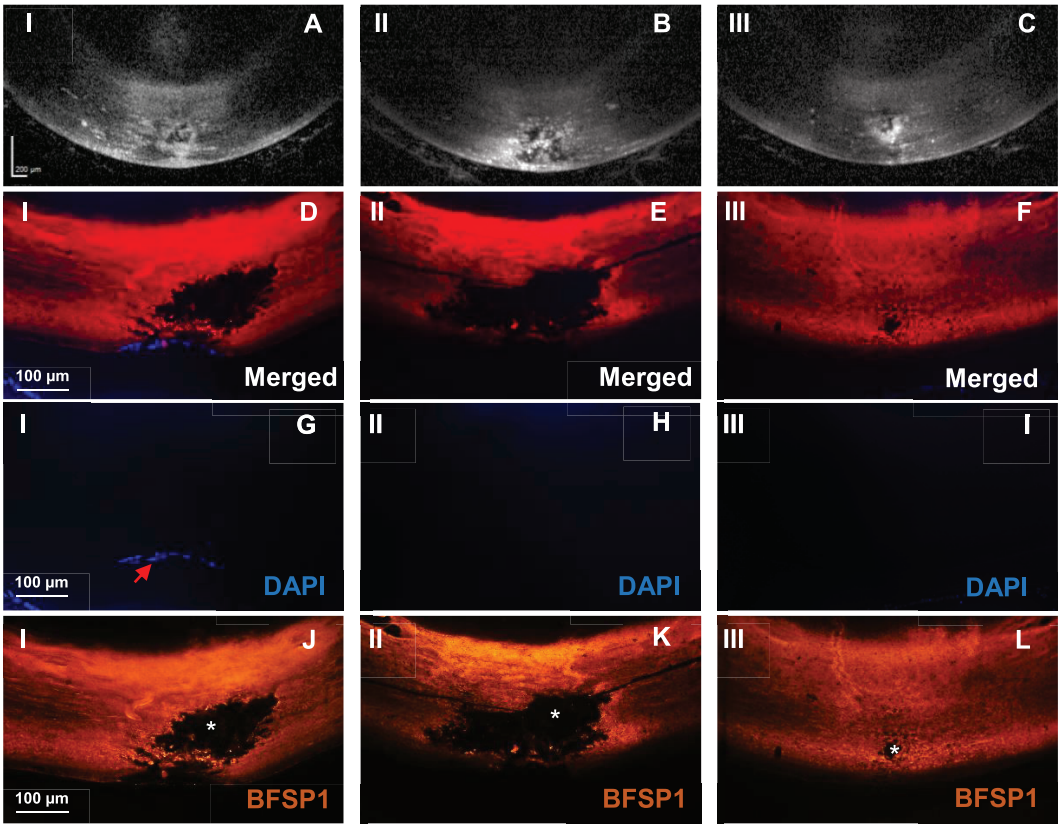

FIG. 11. Lenticular beaded filament structural protein 1 (BFSP1) distribution within posterior lesions of 2 Gy irradiated samples, 19–20 months postirradiation. Female WT (I) and male mutants (II and III). Panels A–C: OCT image. Panels D–F: Merged IHC image. Panels G–I: DAPI. Panels J–L: BFSP1. For panels D–L, magnification = 20×. Red arrows indicate misplaced nuclei. White stars indicate correlates of SF-areas in OCT (tomography not necessarily matching the section).

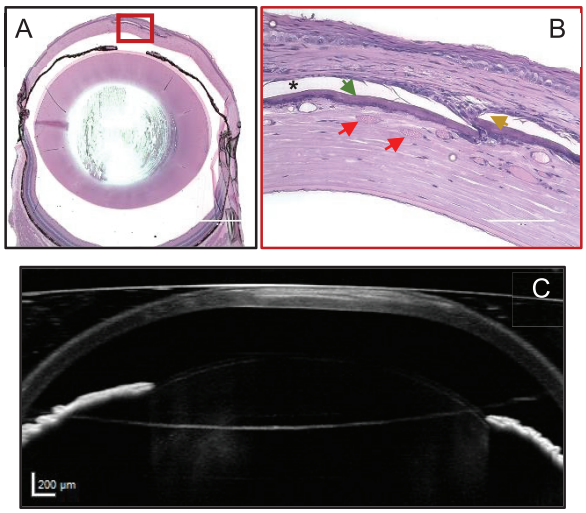

FIG. 12. Corneal alterations. Panel A: Eye histology of a female mutant at 20 months after 0.5 Gy irradiation (4×). Corneal atrophy of marked corneal region in A. Panel B: Blood vessels (red arrows), pseudo basal lamina (green arrow), misguided corneal epithelial cells (yellow arrow) and clefts within the dystrophic structure (black star) (40×). Panel C: Optical coherence tomography of the same eye 17.5 months postirradiation.

A scattering score including anterior and posterior scattering components of both lenses (SS_{AP}) was calculated for the 2 Gy cohort additionally (Fig. 15B), but only for one third of the cohort in which lesion OCT data of all four possible lesion sites was readily available (therefore, low explanatory power). Nonetheless, an increase of SS_{AP} beyond 2 did not result in decreased mean spatial

TABLE 5
Corneal Alterations (OCT-Verified) in 2 Gy Irradiated Mice Compared to Controls, 18.5 Months Postirradiation

Dose	Group	No. of clouded corneas	No. of all lenses	Fraction (%)	Median corneal index
0 Gy	WT/m	0	6	0	0
	WT/f	6	14	42.9	0
	Mut/m	0	7	0	0
	Mut/f	3	10	30	0
2 Gy	WT/m	3	24	12.5	0
	WT/f	2	12	16.7	0
	Mut/m	0	27	0	0
	Mut/f	19	21	90.5	5

Notes. Clouded corneas as fraction of all investigated lenses of each group. Cornea index as combined clouding of both corneas on a scale (0; 6).

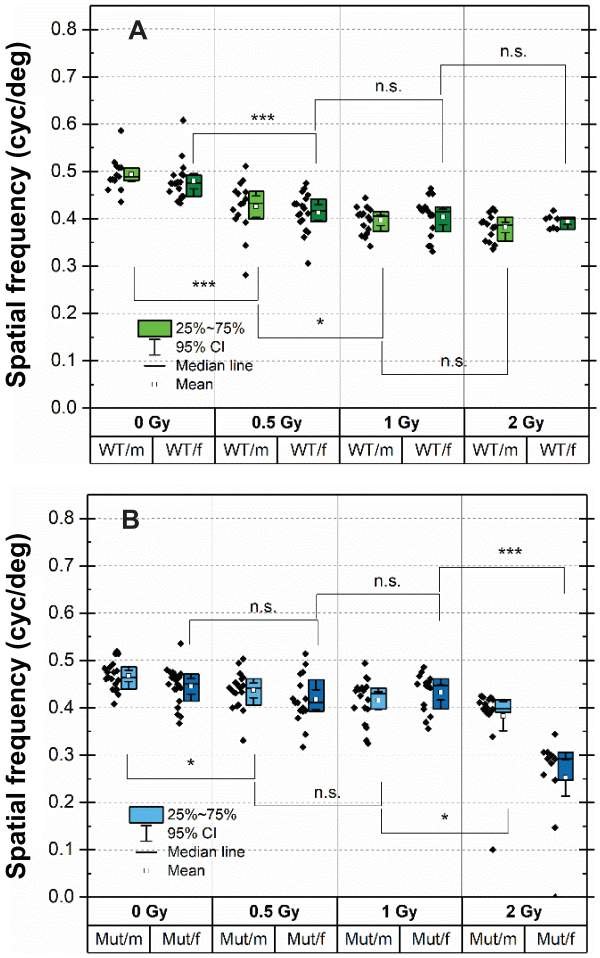

FIG. 13. Visual acuity, 18–19 months postirradiation, of wild-type mice (panel A), and heterozygous *Ercc2* mutant mice (panel B). Significances inserted were determined by Mann-Whitney test.

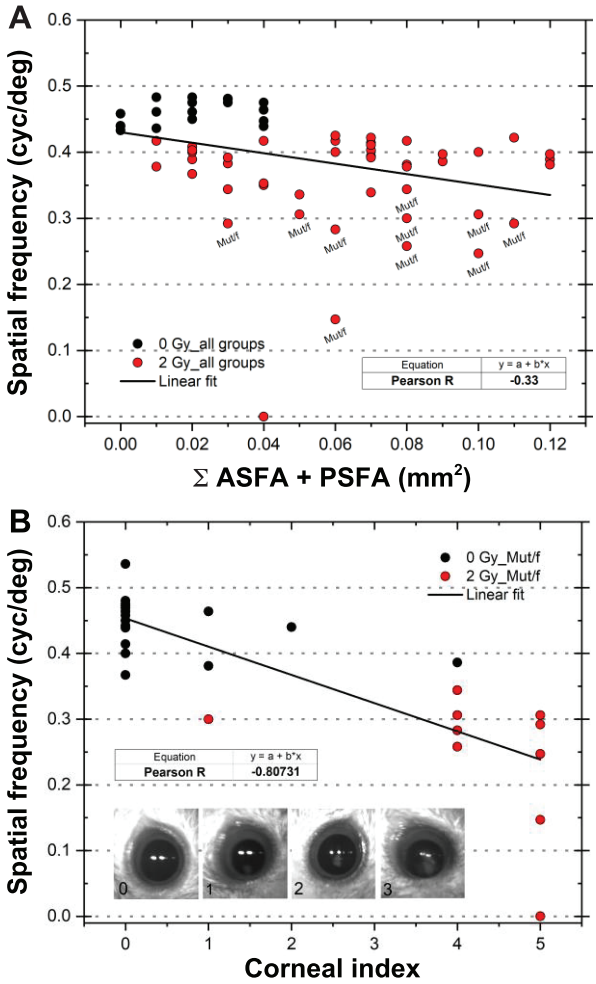

FIG. 14. Visual acuity of each examined animal of the 2 Gy irradiated cohort and associated controls in relationship to the lenticular and corneal alterations within both eyes (19 months postirradiation). Spatial frequency vs. summarized size of the anterior and posterior signal-free area (ΣASFA + PSFA) in both eyes; female mutants labeled (panel A). Spatial frequency of female mutants vs. combined corneal clouding (corneal index) of both eyes of the animal according to Scheimpflug-based corneal classification depicted within (e.g., animal with combined value of 5 may possess a cornea with a value of 2 and another with a value of 3). Panel B: Female mutant controls of all cohorts.

frequencies, which could hint at the lower impact of anterior lesions.

DISCUSSION

In the current study, we assessed radiation-induced alterations within the eye and their effect on mouse vision. In addition, we observed *in vivo* patterns across OCT images and matched them to postmortem lesions within histological sections. Lacking any doubt, qualitative posterior *in vivo* classification was exclusively qualitative and may possibly be strengthened by signal quantization/automatization and the designation improved by blinding. Nevertheless, the scoring was conducted at all times by a single individual according to defined criteria, as discussed above, and the differences between the controls and the irradiated lenses were convincing, and also delivered a clue to explain the differences of age-induced and radiation-induced PSCs. As demonstrated by histology, the SF/S-type lesion was more fragmented and composed of smaller, more deranged fiber cells, cellular debris, and occasionally higher levels of pseudoepithelial cells than the SF-type (Fig. 9). The aforementioned components were most likely responsible for the higher levels of scattering within the posterior lesion recordable via OCT. By quantification of the ASFA/PSFA, we were also able to observe that increased fiber cell swelling and potential liquefied protein reservoirs, respectively, were distinctive lenticular features after irradiation (Figs. 2B and 5B). The PSFAs were surprisingly not dose-dependent at the end of the observation time. Possible differences could occur in a time-dependent manner, due to possible dose-dependent rearrangements within the lesions. A much higher PSFA of the 2 Gy cohort at an earlier time point could indicate this and was also a strong indication of the dynamic nature of radiation-induced lesions. Any appearance of an ASFA *in vivo*, however, was a clear indication of a 2 Gy dose.

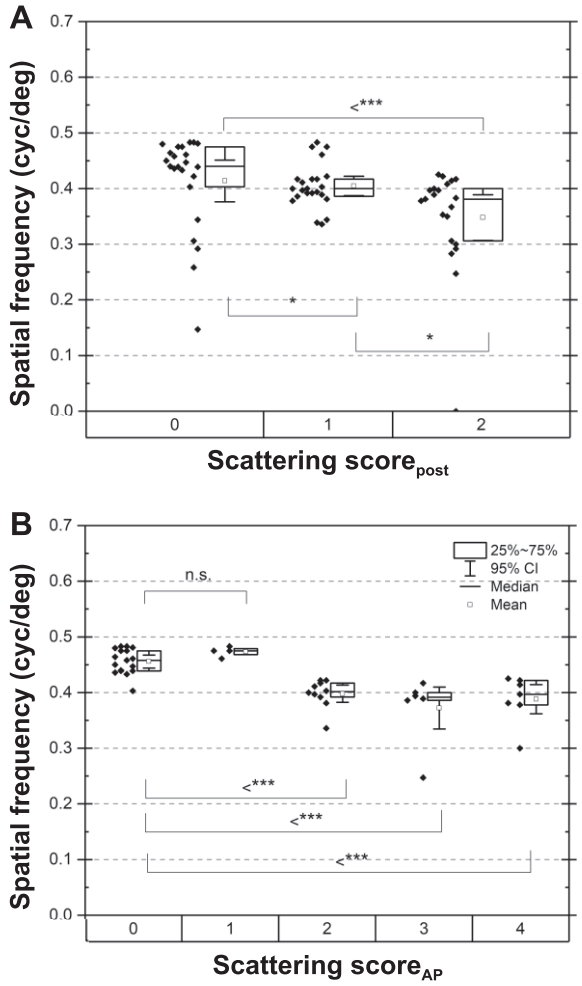

FIG. 15. Spatial frequencies of 2 Gy irradiated mice and 21 controls correlated with scattering properties of investigated lesions. Panel A: Spatial frequency vs. posterior scattering score (SS_{post}) of every mouse. Panel B: Spatial frequency vs. whole lens scattering score (SS_{WL}) if entire information is provided for both lenses of the examined mice. Significances were determined using Mann-Whitney test.

Whether the observed rearrangements were late lenticular regeneration attempts or not, fragmentation to SF/S- or evolvement to S-type lesion was characterized by additional scattering areas, either as a layer in parallel to the posterior capsule, or as an area around the PSFA decreasing in size. These findings were highly relevant for the evaluation of lesions regarding histology in general: in histology, the examiner is completely unaware of the optophysical properties of the lesions. A large cavern filled with liquefied proteins or a mass of few increased fiber cells may appear to be a severe PSC, but *in vivo*, this lesion appears to possess no scattering effect at all. A PSC in histology (like the SF-type *in vivo*), need therefore not be pathological from the vision-focused perspective. In reverse, a wholly innocuous alteration in histology may comprise a severe S-type lesion *in vivo*.

Bearing these facts in mind, it appeared rather futile to compare PSC/AC frequencies directly with OCT-based results. Because a SF-phenotype *in vivo* could comprise just an irregularity in histology, the differences between the results are striking (Figs. 2A and 5A compared with Fig. 7A and B). In particular, the anterior analysis of controls *in vivo* deviated drastically from the histological analysis. The time offset of 1.5 months between *in vivo* and postmortem analysis may have had a non-negligible influence.

However, analysis via histology revealed that 12 months postirradiation, only mice exposed to 2 Gy formed significantly more PSCs (Table 3, OR = 14.44; $P = 0.002$), implying a threshold assumption for radiation-induced PSCs of 2 Gy. Anterior lesions, on the other hand, displayed no significant increase based on histology, 12 months postirradiation. Optically, the threshold-driven occurrence of PSCs was apparently replaced by a linear occurrence of PSCs 20 months postirradiation. Accordingly, 1 Gy and 2 Gy irradiated mice displayed increased odds ratios (OR = 6.4, $P = 0.01$; and OD = 24.6, $P = 0.001$), while 0.5 Gy irradiated animals did not (although 27 lenses were compared to 25 controls). This finding was not in accordance with previous experiments conducted on animals of the same genetic background with a lower dose rate of 0.063 Gy/min (*37*).[5] There, odds ratio for the pooled 0.5 Gy cohort was 9.28. In fact, inversed dose-rate effects were observed in the lens epithelium before (*34*). Therefore, increased lesion frequencies/odds ratios in mice of the same genetic background after 0.5 Gy irradiation at a dose rate of 0.063 Gy/min could be derived from the substantiated epithelial damage. Fewer PSCs after irradiation at a dose rate of 0.3 Gy/min would buttress the hypothesis of an inversed lenticular effect on adult murine lenses at the given dose level.

ACs followed the same occurrence pattern as their posterior counterparts with significantly increased odds ratios across the 1 Gy and 2 Gy cohort 20 months postirradiation (OR = 8.4, $P = 0.01$; and OD = 17.2, $P = 0.001$). However, despite the collection of all histological mid-sagittal sections containing the suture convergence at the anterior and the posterior pole, it remains possible that some actual PSCs or ACs were not revealed in the analysis (thus compromising the calculated odds ratios).

PSCs were similar in morphology as previously described by others, e.g., (*7*). It is remarkable that the arrival of migratory fiber cells to the posterior pole was shifted depending upon dose. First migratory fiber cells accumulating to posterior pseudoepithelia were observed 4 months after 2 Gy irradiation (Fig. 7A). This was far earlier than in Columbia-Sherman albino rats that received 2 Gy X-ray irradiation at the age of 4 weeks. Worgul *et al.* discovered first nuclei at the posterior suture approximately 15 months postirradiation and none at all after irradiation at lower doses (*35*). Lower-doses of radiation slowed the aberration

[5] This article was accepted after typesetting, therefore this reference is out of order.

process down or reduced its frequency. However, first posterior pseudoepithelial cells were provable 12 months after 0.5 or 1 Gy irradiation, and across controls as well.

Plaques of ACs displayed no shape similar to the descriptions found in the literature (*17*). Epithelial cells that accumulated at the pole were not spindle-shaped and were instead rather polygonal (Fig. 8A).

Visual acuity was much less reduced than in mice hailing the same genetic background irradiated at neonatal age (P2) and examined 9 months postirradiation, as shown by Maisel (*21*). Nearly all irradiated neonatal mice displayed inner cortical cataracts and dystrophy of the retina. Thus, the smaller reduction of visual acuity in the irradiated adult mice may possibly have been an expression of the still-intact retina of the irradiated mice. (Retinae in none of the irradiated groups was affected compared to the controls. See Supplementary Fig. S1; https://doi.org/10.1667/RADE-20-00163.1.S5). Wherever the cornea as part of the optic apparatus was affected however, visual acuity dropped inevitably (see Fig. 14B, female mutants).

From deficient correlations of visual acuity and the signal-free area it can be concluded that signal-free areas are of negligible relevance for mouse vision (Fig. 14A). If one understands these findings as representative measures for all alterations at the anterior and posterior pole, they were possibly not valid enough. In fact, many of the irradiated mice with the same combined signal-free area performed worse than the controls, and many mice performed similarly, but had an increased signal-free area. Therefore, other variables come into play, in terms of corneal damage (Fig. 14B). Our team was able to demonstrate that corneal damage (e.g., distinctive in female mutants) correlates quite convincingly with the measured visual acuity and outweighs the lenticular damage. For better correlation attempts, a reliable way must be identified to produce OCT images possessing coherent gray values, to assess the influence of the actual scattering in the lens with the outcomes in the virtual drum. The dyadic lenticular scattering score (Fig. 15A) verified that data separation by a rather simple quantity incorporating the scattering features of the observed PSCs could be convincing. That an extension of this score to AC (SS_{AP}) did not yield further data separation may support the idea that the posterior subcapsular lens cortex is necessary as more crucial for light convergence than the anterior lens where the light falls in.

The few selected lesion sides demonstrating crystallin and BFSP1 distribution were the first contribution to specifically local protein changes at the posterior cataract. They supported the hypothesis from histological analysis that swollen fiber cells and reservoirs are actual different entities. It became manifest in the current study that reservoirs (signal-free areas in OCT) were indeed devoid of α- and γ-crystallins as well as BFSP1 because no antibody could interact with conformation-intact molecules (Figs. 10 and 11J–L). Therefore, we assume that these reservoirs contain degraded (liquefied) proteins. Swollen fiber cells appeared not to differ from regular bulky fiber cells in terms of their irregularities, but possibly in terms of their fragmented mature lesions (compare Fig. 10, panel J with panel L). However, crystallin-depleted reservoirs scatter less infrared light (of the OCT) than surrounding fiber cells. Apparently less crystallin and BFSP1 in the nuclei-carrying fiber cells at the poles suggest radical radiation-induced changes of the expression patterns in these cells.

CONCLUSION

In this study, we established an OCT-based *in vivo* approach to classify anterior and posterior lens alterations, and revealed optophysical differences between radiation- and age-induced cataracts (based on lenticular scattering/visual acuity correlations of controls and irradiated mice). Overall, radiation-induced cataracts displayed a larger area of swollen fiber cells and liquefied proteins and more scattering-associated phenotypes at the same time, while scattering *in vivo* phenotypes were less present in controls. We see not only a basic principle for radiation exposure diagnostics demonstrated, but reason that this could also be an important contribution in determining the crucial changes within a subcapsular lesion responsible for impairing the light-converging function of the crystallin lens. After all, we could reject the notion of a static PSC by monitoring the disappearance of swollen fiber cells and liquefied protein reservoirs which helps to understand the cataract mechanism beyond first fiber cell swelling and pseudoepithelium formation. As it plays out, lenticular subcapsular lesions did not correlate unambiguously with minor dose-dependent reductions of visual acuity.

The current study demonstrated clearly that accelerated occurrence of both PSCs and ASCs together are a feature of murine lenses exposed to gamma rays. Furthermore, our team demonstrated why the question regarding the deterministic or stochastic nature of the cataract occurrence is still such a controversial one: in the middle of our mice's life, investigations suggest a threshold model for PSC occurrence. Near the end of their lifetime, a linear dependency appears to be more palpable. Both appear to be true. Latency is a dose-dependent quantity and tends to favor a threshold model as the chosen observation time becomes smaller. From a purely mechanistic perspective, a long latency relativizes this conclusion to a point where even low doses may induce significantly increased occurrences of PSCs. This fact, and the results on vision impairment, further the scientific community's understanding of radiation effects on the lens and, together with future similar studies, may help to improve current radiation protection guidelines.

SUPPLEMENTARY INFORMATION

Fig. S1. Examples of representative retinal conditions in male WT B6C3F1 mice, 20 months after irradiation at P70. Panel A: Sham-irradiated. Panel B: 0.5 Gy irradiated. Panel C: 1 Gy irradiated. Panel D: 2 Gy irradiated.

Video S1. A representative OCT volume scan of a lenticular N-type in a male B6RCF1 mouse, 17.5 months after sham irradiation.

Video S2. A representative OCT volume scan of an S-type posterior lenticular lesion in a male B6RCF1 mouse at 18.5 months after 1 Gy irradiation.

Video S3. A representative OCT volume scan of an SF-type posterior lenticular lesion in a male B6RCF1 mouse at 18.5 months after 1 Gy irradiation.

Video S4. A representative OCT volume scan of an SF/S-type posterior lenticular lesion in a B6C3F1 mouse at 18.5 months after 1 Gy irradiation.

ACKNOWLEDGMENTS

We thank Erika Bürkle and Monika Stadler for their excellent technical assistance. The German Mouse Clinic received funding from the German Federal Ministry of Education and Research (Infrafrontier Grant No. 01KX1012 to MHdA). We also thank the entire LDLensRad consortium for suggestions and encouragement. This study was financed by the LDLensRad project, which received funding from the Euratom Research and Training Programme, 2014–2018, under Grant Agreement No. 662287. This publication reflects only the authors' view. Responsibility for the information and views expressed herein lies entirely with the authors. The European Commission is not responsible for any use that may be made of the information it contains.

Received: July 2, 2020; accepted: January 5, 2021; published online: February 25, 2021

REFERENCES

1. Little MP. A review of non-cancer effects, especially circulatory and ocular diseases. Radiat Environ Bioph 2013; 52:435–49.
2. Ainsbury EA, Bouffler SD, Dorr W, Graw J, Muirhead C, Edwards AA, et al. Radiation cataractogenesis: A review of recent studies. Radiat Res 2009; 172:1–9.
3. Worgul BV, Kundiyev YI, Sergiyenko NM, Chumak VV, Vitte PM, Medvedovsky C, et al. Cataracts among Chernobyl clean-up workers: Implications regarding permissible eye exposures. Radiat Res 2007; 167:233–43.
4. Azizova TV, Hamada N, Grigoryeva ES, Bragin EV. Risk of various types of cataracts in a cohort of Mayak workers following chronic occupational exposure to ionizing radiation. Eur J Epidemiol 2018; 33:1193–204.
5. Urban Jr RC, Cotlier E. Corticosteroid-induced cataracts. Surv Ophthalmol 1986; 31:102–10.
6. Delcourt C, Cristol J-P, Tessier F, Leger CL, Michel F, Papoz L, et al. Risk factors for cortical, nuclear, and posterior subcapsular cataracts: The POLA study. Am J Epidemiol 2000; 151:497–504.
7. Eshaghian J, Streeten BW, Leger CL, Michel F, Papoz L. Human posterior subcapsular cataract: An ultrastructural study of the posteriorly migrating cells. Arch Ophthalmol-Chic 1980; 98:134–43.
8. Streeten BW, Eshaghian J. Human posterior subcapsular cataract: A gross and flat preparation study. Arch Ophthalmol 1978; 96:1653–8.
9. Hanna C, O'Brien JE. Lens epithelial cell proliferation and migration in radiation cataracts. Radiat Res 1963; 19:1–11.
10. Stefano I de, Tanno B, Giardullo P, Leonardi S, Pasquali E, Antonelli F, et al. The Patched 1 tumor-suppressor gene protects the mouse lens from spontaneous and radiation-induced cataract. Am J Pathol 2015; 185:85–95.
11. Srinivasan Y, Lovicu FJ, Overbeek PA. Lens-specific expression of transforming growth factor beta1 in transgenic mice causes anterior subcapsular cataracts. J Clin Invest 1998; 101:625–34.
12. Lovicu FJ, Schulz MW, Hales AM, Vincent L, Overbeek PA, Chamberlain Cg, et al. TGFbeta induces morphological and molecular changes similar to human anterior subcapsular cataract. Br J Ophthalmol 2002; 86:220–6.
13. Eldred JA, Dawes LJ, Im Wormstone. The lens as a model for fibrotic disease. Philos Trans R Soc Lond B Biol Sci 2011; 366:1301–19.
14. Imaizumi T, Kurosaka D, Tanaka U, Sakai D, Fukuda K, Sanbe A. Topical administration of a ROCK inhibitor prevents anterior subcapsular cataract induced by UV-B irradiation. Exp Eye Res 2019; 181:145–9.
15. Font RL, Brownstein S. A light and electron microscopic study of anterior subcapsular cataracts. Am J Ophthalmol 1974; 78:972–84.
16. Hatae T, Ishibashi T, Yoshitomi F, Shibata Y. Immunocytochemistry of types I-IV collagen in human anterior subcapsular cataracts. Graef Arch Clin Exp 1993; 231:586–90.
17. Lovicu FJ, Steven P, Saika S, McAvoy JW. Aberrant lens fiber differentiation in anterior subcapsular cataract formation: A process dependent on reduced levels of Pax6. Invest Ophth Vis Sci 2004; 45:1946–53.
18. Pau H, Novotny GE. Ultrastructural investigations on anterior capsular cataract. Cellular elements and their relationship to basement membrane and collagen synthesis. Graef Arch Clin Exp 1985; 223:41–6.
19. Stewart FA, Akleyev AV, Hauer-Jensen M, Hendry JH, Kleiman NJ, Macvittie TJ, et al. ICRP publication 118: ICRP statement on tissue reactions and early and late effects of radiation in normal tissues and organs–threshold doses for tissue reactions in a radiation protection context. Ann ICRP 2012; 41:1–322.
20. Hamada N, Azizova TV, Little MP. An update on effects of ionizing radiation exposure on the eye. Br J Radiol 2020; 93:20190829.
21. Maisel H. The ocular lens: Structure, function, and pathology. New York: Marcel Dekker Inc.; 1985.
22. Gajewski AK, Majewska K, Slowikowska MG, Chomiczewski K, Kulig A. Types and rate of cataract development in mice irradiated at different ages. Radiat Res 1977; 71:471–80.
23. Kunze S, Dalke C, Fuchs H, Klaften M, Rossler U, Hornhardt S, et al. New mutation in the mouse Xpd/Ercc2 gene leads to recessive cataracts. Plos One 2015; 10:e0125304.
24. Dalke C, Neff F, Bains SK, Bright S, Lord D, Reitmeir P, et al. Lifetime study in mice after acute low-dose ionizing radiation: A multifactorial study with special focus on cataract risk. Radiat Environ Bioph 2018; 57:99–113.
25. Pawliczek D, Dalke C, Fuchs H, Gailus-Durner V, Hrabe de Angelis M, Graw J, et al. Spectral domain-Optical coherence tomography (SD-OCT) as a monitoring tool for alterations in mouse lenses. Exp Eye Res 2020; 190:107871.
26. Puk O, Angelis MH de, Graw J. Longitudinal fundus and retinal studies with SD-OCT: A comparison of five mouse inbred strains. Mamm Genome 2013; 24:198–205.
27. Puk O, Dalke C, Calzada-Wack J, Ahmad N, Klaften M, Wagner S, et al. Reduced corneal thickness and enlarged anterior chamber in a novel ColVIIIa2G257D mutant mouse. Invest Ophth Vis Sci 2009; 50:5653–61.
28. Prusky GT, Alam NM, Beekman S, Douglas RM. Rapid quantification of adult and developing mouse spatial vision using

a virtual optomotor system. Invest Ophth Vis Sci 2004; 45:4611–16.

29. Lehmann K, Schmidt KF, Lowel S. Vision and visual plasticity in ageing mice. Restor Neurol Neurosci 2012; 30:161–78.

30. Neff F, Flores-Dominguez D, Ryan DP, Horsch M, Schroder S, Adler T, et al. Rapamycin extends murine lifespan but has limited effects on aging. J Clin Invest 2013; 123:3272–91.

31. Xie Q, McGreal R, Harris R, Gao CY, Liu W, Reneker L, et al. Regulation of c-maf and a-crystallin in ocular lens by fibroblast growth factor signalling. J Biol Chem 2016; 291:3947–58.

32. Altman DG. Practical statistics for medical research. Florida: CRC Press; 1990.

33. Pagano M, Gauvreau K. Principles of biostatistics. Belmont, CA: Brooks/Cole; 2000.

34. Barnard SGR, McCarron R, Moquet J, Quinlan R, Ainsbury E. Inverse dose-rate effect of ionising radiation on residual 53BP1 foci in the eye lens. Sci Rep 2019; 9:1–8.

35. Worgul BV, Merriam GR, Medvedovsky C. Accelerated heavy particles and the lens II. Cytopathological changes. Invest Ophth Vis Sci 1986; 27:108–14.

36. Pawliczek D, Fuchs H,Gailus-Durner V, Angelis M, Graw J, Dalke C. Ionising radiation causes vision impairment in neonatal B6C3F1 mice. Experimental Eye Res 2021; 204:108432. doi: 10.1016/j.exer.2020.108432.

37. Kunze S, Cecil A, Prehn C, Möller G, Ohlmann A, Wildner G, et al. Posterior subcapsular cataracts are a late effect after acute exposure to 0.5 Gy ionizing radiation in mice. Int J Radiat Biol 2021; 97:4, 529–540. doi: 10.1080/09553002.2021.1876951.